Observed influence of North Pacific SST anomalies on the atmospheric circulation

Claude Frankignoul, Nathalie Sennéchael

Observed Influence of North Pacific SST Anomalies on the Atmospheric Circulation

CLAUDE FRANKIGNOUL AND NATHALIE SENNÉCHAEL

LOCEAN/IPSL, Université Pierre et Marie Curie, Paris, France

(Manuscript received 21 March 2006, in final form 22 June 2006)

ABSTRACT

A lagged maximum covariance analysis (MCA) of monthly anomaly data from the NCEP–NCAR reanalysis shows significant relations between the large-scale atmospheric circulation in two seasons and prior North Pacific sea surface temperature (SST) anomalies, independent from the teleconnections associated with the ENSO phenomenon. Regression analysis based on the SST anomaly centers of action confirms these findings. In late summer, a hemispheric atmospheric signal that is primarily equivalent barotropic, except over the western subtropical Pacific, is significantly correlated with an SST anomaly mode up to at least 5 months earlier. Although the relation is most significant in the upper troposphere, significant temperature anomalies are found in the lower troposphere over North America, the North Atlantic, Europe, and Asia. The SST anomaly is largest in the Kuroshio Extension region and along the subtropical frontal zone, resembling the main mode of North Pacific SST anomaly variability in late winter and spring, and it is itself driven by the atmosphere. The predictability of the atmospheric signal, as estimated from cross-validated correlation, is highest when SST leads by 4 months because the SST anomaly pattern is more dominant in the spring than in the summer. In late fall and early winter, a signal resembling the Pacific–North American (PNA) pattern is found to be correlated with a quadripolar SST anomaly during summer, up to 4 months earlier, with comparable statistical significance throughout the troposphere. The SST anomaly changes shape and propagates eastward, and by early winter it resembles the SST anomaly that is generated by the PNA pattern. It is argued that this results via heat flux forcing and meridional Ekman advection from an active coupling between the SST and the PNA pattern that takes place throughout the fall. Correspondingly, the predictability of the PNA-like signal is highest when SST leads by 2 months. In late summer, the maximum atmospheric perturbation at 250 mb reaches 35 m K^{-1} in the MCA and 20 m K^{-1} in the regressions. In early winter, the maximum atmospheric perturbation at 250 mb ranges between 70 m K^{-1} in the MCA and about 35 m K^{-1} in the regressions. This suggests that North Pacific SST anomalies have a substantial impact on the Northern Hemisphere climate. The back interaction of the atmospheric response onto the ocean is also discussed.

1. Introduction

In the 1960s and early 1970s, it was often speculated on the basis of contemporary correlations that North Pacific sea surface temperature (SST) anomalies have an influence on the large-scale atmospheric circulation on the seasonal time scale (e.g., Namias 1963). However, Davis (1976) showed that the cross correlation between SST and sea level pressure (SLP) anomalies reflected the atmosphere driving the ocean. This was consistent with the stochastic climate model of Frankignoul and Hasselmann (1977), who demonstrated that large contemporary correlations between SST and the atmosphere were well explained by the passive response of the SST to the atmospheric forcing. At the same time, Namias (1976) showed that summer SST anomalies in the Aleutian area were significantly correlated with the atmospheric circulation in the following fall, which is more indicative of an SST influence. Similar results were found by Davis (1978), who also showed that winter SLP anomalies over the North Pacific could be predicted from fall SST anomalies. SLP was an equally effective predictor, however, so that the role of the local air–sea interactions was uncertain. Barnett (1981) suggested that SST anomalies in the equatorial Pacific may have been the origin of both correlations. The strong teleconnections between tropical and extratropical latitudes were emphasized by Horel and Wallace (1981), and the interest of researchers

Corresponding author address: Claude Frankignoul, LOCEAN/IPSL, Université Pierre et Marie Curie, Paris 6, case 100, 4 place Jussieu, 75252 Paris CEDEX 5, France.
E-mail: cf@lodyc.jussieu.fr

mostly shifted to the climatic influence of the El Niño–Southern Oscillation (ENSO) phenomenon. This was also fuelled by the weak (and model-dependent) influence of North Pacific SST anomalies found in the early prescribed change experiments with atmospheric general circulation models (GCMs; see review in Frankignoul 1985), which contrasted with a large sensitivity to tropical SST anomalies.

By the late 1990s, use of larger ensembles of GCM simulations had nonetheless suggested that midlatitude SST anomalies could have a significant influence on the atmosphere, although the amplitude was modest (of the order of 10–20 m per K anomaly at 500 hPa) and the response was somewhat model dependent (see review in Kushnir et al. 2002). The response was very sensitive to the climatological state and the SST anomaly location. Hence, an SST anomaly could lead to a drastically different response from one month to the next because of the changes in the background flow (Peng et al. 1997). This occurs because the response critically depends on the interaction between the direct baroclinic response to the SST-induced heating and the transient eddies, which are sensitive to the climatology (Peng and Whitaker 1999). The internal variability of the atmosphere is also largely maintained by the transient eddy forcing, hence there is evidence that the SST anomalies tend to shift the frequency of occurrence of some of the modes of internal variability, rather than create new modes of variability (Peng and Robinson 2001; Cassou et al. 2004).

Once they have been generated, the extratropical SST anomalies are generally damped by a negative turbulent heat flux feedback (Frankignoul et al. 1998; Frankignoul and Kestenare 2002), thereby modulating the heat exchanges between the ocean and the atmosphere. The SST anomaly influence on the atmospheric circulation has been difficult to detect in the observations. Czaja and Frankignoul (1999, 2002) showed that SST anomalies in the North Atlantic had a significant influence on the large-scale atmospheric circulation in early winter and late spring. Whether SST anomalies in the North Pacific similarly influence the tropospheric circulation during certain months has been speculated (e.g., Zhang et al. 1998; Tanimoto et al. 2003) but not demonstrated, perhaps because the strong signal associated with the ENSO phenomenon tends to mask other influences. Using high-resolution observations, Nonaka and Xie (2003) detected a strong local SST influence on the planetary boundary layer wind over the Kuroshio and its extension, but the link with the large-scale atmospheric circulation was not established. Nonetheless, additional evidence points to an active role of the North Pacific SST anomalies. For instance, the potential predictability of precipitation over the United States seems to depend, albeit to a small extent, on SST anomalies in the North Pacific, in particular during early fall (Lau et al. 2002). Based on the lagged correlation between observed SST and SLP in the Kuroshio Extension region, Liu and Wu (2004) suggested that there was a possible atmospheric response to SST during fall, although statistical significance was very small.

Despite the lack of observational evidence, it has often been speculated that North Pacific SST anomalies have an influence on the atmosphere that could feed back on the ocean and generate decadal variability. For instance, Latif and Barnett (1994) suggested that changes in the subtropical gyre strength generate SST anomalies that are enhanced by a positive heat flux feedback, but then change polarity because of a delayed negative feedback resulting from the wind stress curl response to the SST anomalies, which reversed the initial gyre perturbation after adjustment via Rossby wave propagation. Further investigation found little evidence of the hypothesized ocean–atmosphere feedback loop, however, suggesting instead that the decadal variability resulted primarily from stochastic Ekman pumping (Seager et al. 2001; Schneider et al. 2002). Coupling a simple ocean model to a statistical atmosphere based on simultaneous correlation patterns between SST and wind stress, Solomon et al. (2003) found that stochastic forcing and midlatitude coupling could generate a substantial decadal variability of the North Pacific subtropical cell, thereby affecting SST in the equatorial Pacific and ENSO. However, when the wind stress patterns were based on the correlation with previous SST, as should be more representative of an atmospheric response, the decadal variability was much weakened.

It is thus timely to reconsider the air–sea coupling in the North Pacific. Here we use the National Centers for Environmental Prediction–National Center for Atmospheric Research (NCEP–NCAR) reanalysis (Kalnay et al. 1996) and investigate the influence of North Pacific SST anomalies on seasonal climate fluctuations, using lagged Maximum Covariance Analysis [MCA, also known as Singular Value Decomposition (SVD) analysis; see, e.g., Bretherton et al. 1992] as in Czaja and Frankignoul (2002). Because of the large multidecadal changes in the North Pacific and the strength of the ENSO influence, care is taken to remove the influence of trends, low frequencies, and the ENSO teleconnections prior to the analysis. A significant relation between the large-scale atmospheric circulation and prior North Pacific SST anomalies is found in late summer and in late fall–early winter. The atmospheric signals

are hemispheric in extent and seem to be predictable with some skill several months in advance. Their possible feedback on the ocean is also briefly discussed since several decadal variability scenarios imply that an active air–sea coupling must be present, at least during part of the year.

2. Data and method

Monthly anomalies of SST in the ice-free areas, SLP, geopotential height at 850, 700, 500, and 250 mb (hereafter Z850, Z500, and Z250), and temperature at 850 mb (T850) were taken from the NCEP–NCAR reanalysis, as well as surface wind stress and turbulent heat flux. The 1958–2003 period was considered at first, but more significant relations between the atmospheric fields and prior SST anomalies were found during the second half of the period, presumably because of the better data quality and the different mean atmospheric state after the "climate shift" of the mid-1970s (e.g., Trenberth and Hurrell 1994). All the results below are thus given for the 1977–2004 period.

To reduce the influence of trends and ultralow-frequency changes, a second-order polynomial was removed by least squares fit from all data. Much of the ENSO influence was also removed by replacing each monthly anomaly $X(t)$ by $X(t) - aN_1(t) - bN_2(t)$, where $N_1(t)$ and $N_2(t)$ are the first two principal components of the monthly SST anomalies in the tropical Pacific between 12.5°N and 12.5°S, and a and b are seasonally varying regression coefficients determined by least squares fit for each variable and grid point, using successive sets of 3 months to get smoothly varying estimates. To take into account the phase asymmetry of the ENSO signal, the regression was done separately for positive and negative values of the principal components. This seems appropriate since the ENSO teleconnection pattern changes between El Niño and La Niña conditions, and depends linearly on the tropical heating in the former case and is independent of it in the latter one (Straus and Shukla 2002). The fractional variance linked to ENSO is substantial even north of 20°N, our reference domain, peaking around 35% for SST and 25% for Z (Fig. 1). Note that the maximum fractional amount of removed variance is larger during boreal winter (about 55% and 35%, respectively), but smaller in summer and fall.

The MCA isolates pairs of spatial patterns and their associated time series by performing a singular value decomposition of the covariance matrix between two fields. Each field is expanded into orthogonal patterns that maximize their covariance, the time series being orthogonal to one another between the two fields. To establish whether the MCA modes are meaningful, statistical significance was estimated using a moving blocks bootstrap approach as in Czaja and Frankignoul (2002): each MCA was repeated 100 times, linking the original SST anomalies with randomly scrambled atmospheric ones based on blocks of two successive years to reduce the influence of serial correlation. The quoted significance levels indicate the percentage of randomized squared covariance (SC) and correlation for the corresponding mode that exceed the value being tested. It is an estimate of the risk of rejecting the null hypothesis (there is no relation between atmospheric and SST anomalies) when it is in fact true, following the standard statistical convention. A smaller significance level indicates the presence of stronger evidence against the null hypothesis.

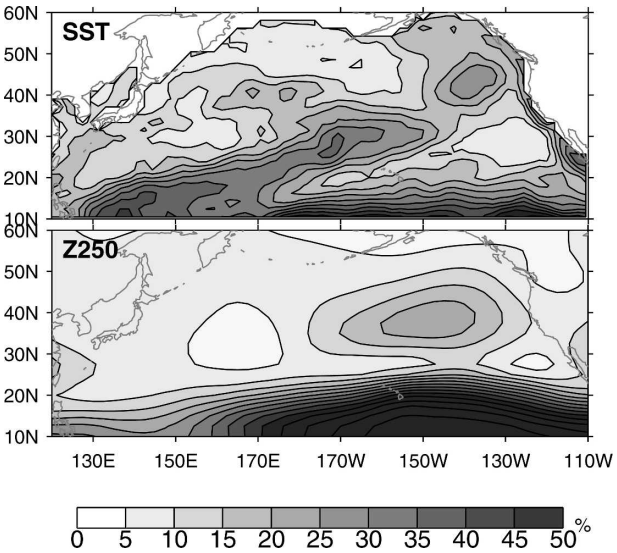

FIG. 1. Amount of fractional variance removed in association with ENSO for (top) SST and (bottom) Z250.

To assess the robustness of the analysis, rotated MCA (Cheng and Dunkerton 1995) was also applied, since it provides pairs of patterns that are no longer orthogonal within each field but are more geographically localized and easier to interpret physically. The varimax rotation turned out to have little influence. Hence only standard MCA results are given. Finally, the predictability of the atmospheric signal was assessed by cross validation, removing successive sets of 3 yr before performing the MCA, and then using the MCA patterns to determine their amplitude in the middle year that was removed.

3. Lagged MCA results for the troposphere

To search for an SST anomaly influence on the atmosphere, the MCA was applied as a function of time

lag and season to monthly SST and geopotential height anomalies in the North Pacific domain, 20°–60°N, 110°E–110°W. Sets of three successive months [months are denoted by the first letter of each month, e.g., January–March (JFM)] were considered with SST leading or lagging. Depending on the season and the lag, the MCA is based on 27 or 28 yr (81 or 84 months). We also performed the MCA with a single month per year, but the sample was too small and the significance too low to improve the time resolution. However, it did not seem that the atmospheric response in the cases discussed below was dominated by a single month.

Throughout the year, the maximum covariance is found at lags ≥ 0 with a peak at lag 1 (SST follows), showing that the dominant air–sea interaction is the forcing of the SST by the atmosphere, consistent with the stochastic climate model of Frankignoul and Hasselmann (1977). The SC and the correlation are highly significant for the first few MCA modes, reflecting the SST anomaly response to the main modes of atmospheric variability. On the other hand, only the first MCA mode was (sometimes) significant at negative lags when SST leads. As the influence of the ocean on the atmosphere is our main focus, the MCA results are summarized in Fig. 2 for the first MCA mode between lag -8 and lag 2, with each tropospheric level being considered separately. There are significant SC and correlation with prior SST anomalies when the atmosphere is taken during late summer (primarily ASO) and during late fall–early winter (primarily OND and NDJ), while there is little hint of SST influence on the tropospheric circulation during the rest of the year. Note that lag –1 is likely to reflect both the atmospheric forcing and its response because of the atmospheric persistence, so that the oceanic influence is best seen at lag ≤ -2.

In late summer (ASO), the SC is maximum and most significant when SST leads by 3 to 5 months. The statistical significance is low in the lower troposphere, but increases with height and is strongest at 250 mb. Note that the mode is seen in the MCA with SLP, but the SC is only 21% and 27% significant at lags –3 and –4, respectively. Why the significance is poor in the lower troposphere remains to be understood.

In late fall–early winter, the signal significance is comparable at each tropospheric level, and the SC peaks and is most significant when the atmosphere is taken in NDJ and SST precedes by 2 to 4 months. In both seasons, the SST anomaly pattern at a given lag remains nearly the same when the geopotential level varies, while the geopotential height pattern changes somewhat as the ground is approached. Hence, nearly identical results were obtained when considering simultaneously all the atmospheric levels in the MCA, instead of a single one as in Fig. 2 (not shown).

As a word of caution, it should be reminded that one would expect some of the MCA modes to yield SC or correlation values that are significant just by chance. Although it will be shown that cross validation and simple regression analysis support the main MCA results, it cannot be assured that they reflect true relationships.

4. SST anomaly influence during late summer

The maximum covariance patterns are illustrated for the summer signal in Fig. 3, which shows homogeneous maps for SST and heterogeneous maps for Z250 in ASO (the regression of both fields onto the SST anomaly time series, which preserve linear relations between the variables) at all lags between –10 and 1 that are 20% significant in both SC and correlation. The SC is strongest at lags 0 and 1, reflecting the forcing of the dominant SST anomaly mode by the atmosphere. Indeed, the SST pattern resembles the first empirical orthogonal function (EOF) of SST anomalies in ASO and SON, while the atmospheric pattern is like the second EOF of Z250 in ASO (not shown).

When the ocean leads, the SC is significant between lag –2 and lag –5, with little change in the maximum covariance patterns (they can be recognized down to lag –7, but significance is lower). Cross validation (Table 1) suggests that the correlation is robust, except at lag –2. The SST anomaly resembles the first SST anomaly EOF from winter (JFM) to early summer (JJA). It has a maximum amplitude along 35°N in the western and central North Pacific, hence in the Kuroshio Extension region and along the subtropical frontal zone, and anomalies of the opposite sign around it. On the other hand, the atmospheric signal does not correspond to a dominant Z250 mode. It has a high reaching 24 m slightly to the northwest of the 0.7-K SST anomaly maximum. The implied sensitivity of 35 m K^{-1} is large, but it is probably overestimated since the MCA maximizes the covariance between SST and the atmosphere. See below for another estimate.

To discuss the air–sea interactions further, we consider lag –4 where the SC, the correlation, the statistical significance, and the cross-validated correlation are the largest. Why lag –4 dominates may be related to the higher signal-to-noise of the SST anomaly pattern that influences the atmosphere. Indeed, the lag – 4 pattern in Fig. 3 accounts for 57% of the SST anomaly variance in AMJ, versus 45% for the lag –3 pattern in MJJ and 32% for the lag –2 pattern in JJA. As the SST anomaly pattern varies very little with lag, the decrease in its

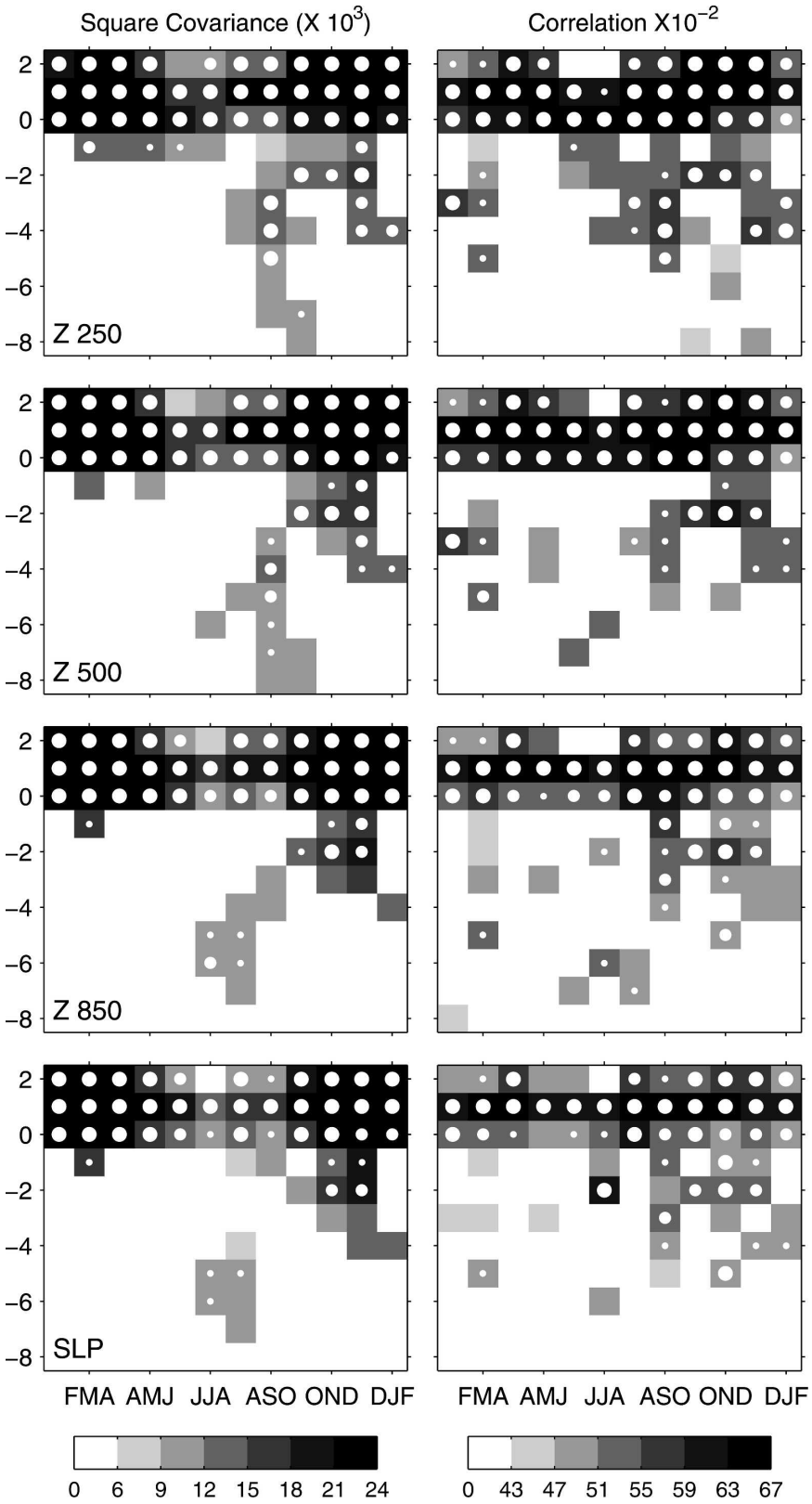

FIG. 2. The (left) SC and (right) correlation as a function of lag (in months, negative when SST leads) and season for the first MCA mode between SST and atmospheric anomalies at different levels for the 1977–2004 period. The SC and correlation are only given when the significance level is better than 20%. Large, medium, and small white dots indicate that the SC or the correlation is significant at the 1%, 5%, and 10% levels, respectively.

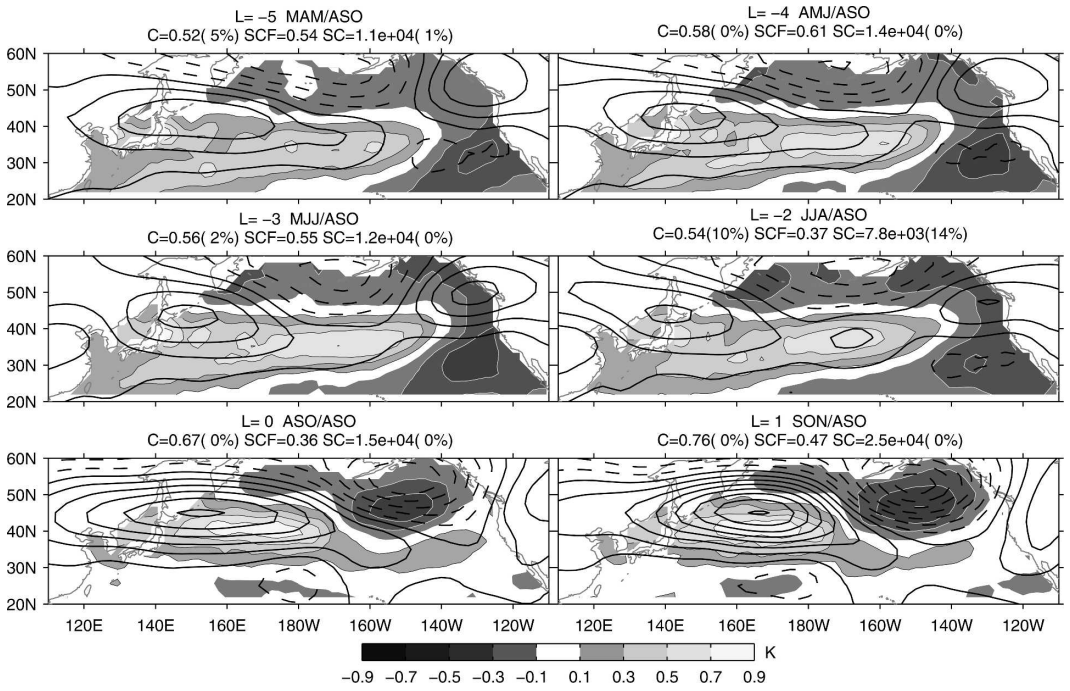

FIG. 3. Maximum covariance pattern for ASO Z250 (contour interval: 6 m with negative values dashed) and SST (scale in K with white contours for negative values and black contours for positive ones) anomalies between lag –5 (SST leads) and lag 1 (SST follows) when the estimated significance level (in parentheses) is better than 20% for both the SC and the correlation. The time series have been normalized so that the figure shows typical amplitudes. The correlation (C) between the MCA time series, the SC fraction (F), and the SC are given for each lag.

relative importance with lag must reflect the appearance of other SST anomaly patterns, consistent with the strong SST anomaly response to the atmospheric forcing that is expected in summer, when the mixed layer is very shallow. The North Pacific SST anomaly variance indeed increases by about 40% between AMJ and MJJ, and then more slowly until JAS.

As shown in Fig. 4 (top), the SST time series (AMJ for each year) show little year-to-year persistence during the first half of the record, but a substantial decadal variability since the. 1990s. The latter resembles that of the SST anomaly in the Kuroshio Extension region of 32°–38°N, 141°E–180°, which was shown by Qiu (2000) to be in part caused by low-frequency changes in the

TABLE 1. Correlation and cross-validated correlation for each of the MCA modes shown at negative lags in Figs. 3, 9, and 12.

Season	Lag	Correlation	Cross validation
ASO	−5	0.52	0.33
	−4	0.58	0.54
	−3	0.56	0.42
	−2	0.54	0.07
SON	−2	0.57	0.38
OND	−2	0.58	0.44
NDJ	−4	0.56	0.36
	−3	0.52	0.36
	−2	0.55	0.43
	−1	0.50	0.39

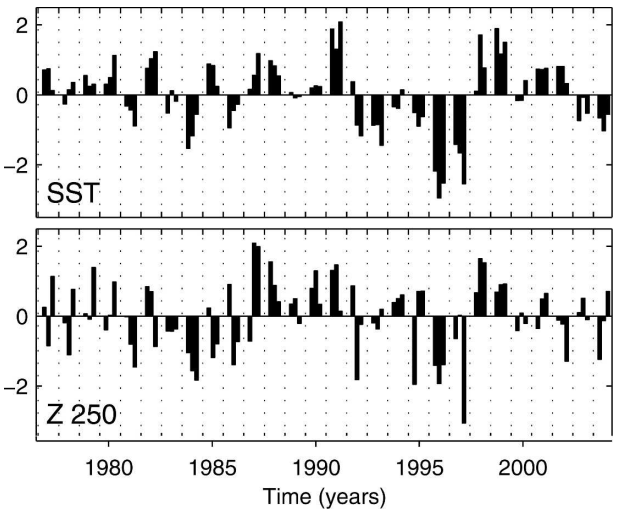

FIG. 4. Time series of the lag –4 MCA mode in Fig. 3 for (top) SST in AMJ and (bottom) Z250 in ASO. Each year is separated by a blank interval.

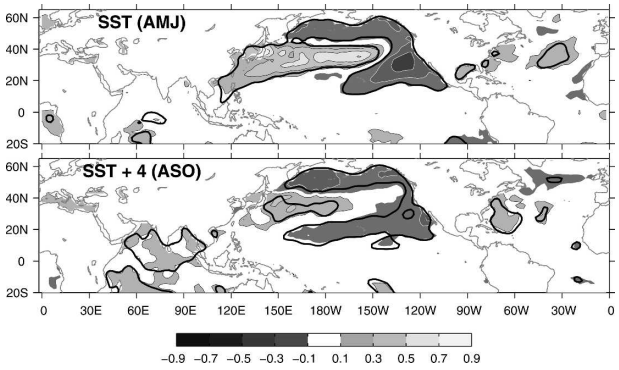

FIG. 5. Regression of the SST anomalies in (top) AMJ and (bottom) 4 months later in ASO onto the lag – 4 AMJ SST time series shown in Fig. 4. White contours are for negative values and black contours for positive ones. The thick lines indicate the estimated 5% significance level.

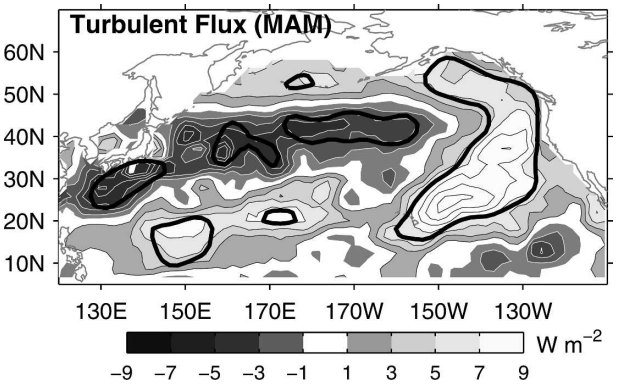

FIG. 6. Regression of the turbulent heat flux anomalies in MAM onto the lag – 4 AMJ SST time series. White contours are for negative values and black contours for positive ones. The thick lines indicate the estimated 5% significance level.

Kuroshio Extension jet, themselves remotely forced by the wind (Qiu 2003). Regressing the SST anomaly fields onto the AMJ SST anomaly time series (Fig. 5, top) shows that the SST anomaly is confined to the North Pacific. However, a small SST anomaly in the North Atlantic and one in the southern Indian Ocean also seem to be significant (statistical significance is based on Bretherton et al. 1999).

The regression of the turbulent heat flux (positive upward) that precedes the AMJ SST anomaly by 1 month (Fig. 6) suggests that the spatial structure of the SST anomaly is primarily determined by heat flux forcing, except in the southwestern part of the domain and near the Kuroshio where the ocean currents strongly contribute (Qiu 2003). Once the SST anomaly has been generated, the associated turbulent heat flux changes sign (not shown, but see Fig. 8 below), thereby slowly damping the SST anomaly. The negative turbulent heat flux feedback is about 10 to 15 W m^{-2} K^{-1}, consistent with the summer values of Frankignoul and Kestenare (2002), who showed that it was tampered by a weak positive radiative feedback. As shown by the regression of the SST anomaly field in ASO (hence 4 months later) onto the AMJ SST anomaly time series (Fig. 5, bottom), the SST anomaly is quite persistent, which explains why an air–sea interaction that presumably takes place during summer can be detected in the MCA by using SST anomalies in the preceding spring. Note that the ASO atmospheric signal may not simply reflect the SST anomaly forcing in ASO, but also that in the preceding months, as the buildup of the atmospheric response may take longer than commonly assumed (Ferreira and Frankignoul 2005). Correspondingly, the SST anomaly decay seen in Fig. 5 is an upper bound of that relevant to the air–sea interaction.

The Z250 times series in Fig. 4 (bottom) is rather well correlated with the SST time series (correlation $C = 0.58$), and it also has some low-frequency variability. Regressing the ASO Z250 anomalies onto the AMJ SST anomaly time series indicates that the atmospheric response pattern is hemispheric in extent, with hints of wave propagation and a substantial, statistically significant, amplitude over North America, the North Atlantic, western Europe, and Asia (Fig. 7, top left). The regression pattern is very similar throughout the troposphere, as illustrated for 700 mb (top right) and SLP (bottom left), which show that the atmospheric signal is primarily equivalent barotropic. However, there is some baroclinicity over the western North Pacific and eastern subtropical Asia, with a broad ridge in the lower troposphere above the positive SST anomaly that tilts westward with height. Significant temperature anomalies are found at low levels, in particular over North America, Europe, and eastern Asia (Fig. 7, bottom right).

To verify that the anomalies in Fig. 3 are not related to ENSO (or that ENSO was well removed), the regression on the AMJ SST time series was also made for the SST and the tropospheric anomalies that were obtained before removing the ENSO signal. There was little difference with the patterns in Figs. 5 and 7, and no significant correlation was found with the SST in the equatorial Pacific, even in lead or lag conditions of a few months.

We attempted to determine which part of the AMJ SST anomaly had the strongest influence on the atmosphere by considering the averaged SST anomaly in boxes centered on the two main centers of action of the SST anomaly pattern, namely 25°–40°N, 140°E–150°W and 25°–35°N, 140°–120°W. Projecting the ASO Z250 anomaly on the two SST time series gave in each case a

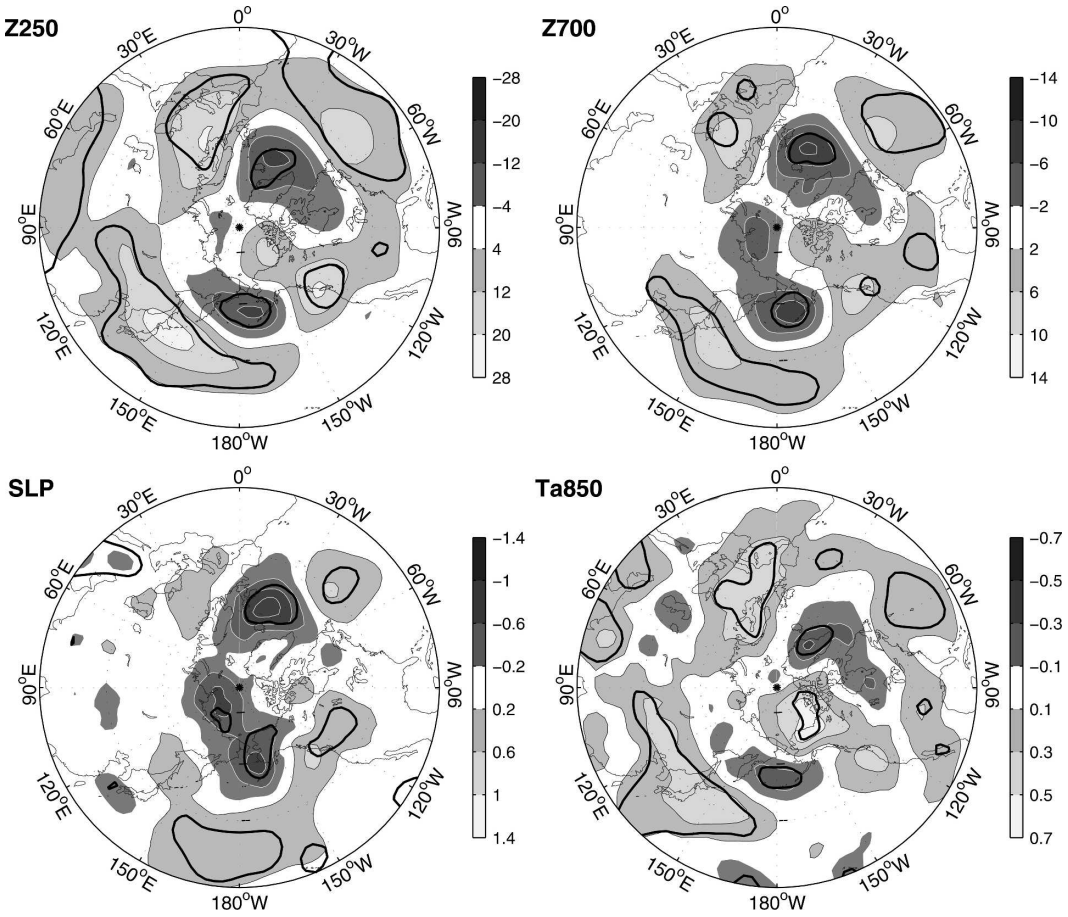

FIG. 7. Same as in Fig. 6, but for regression of the (top left) Z250, (top right) Z700, (bottom left) SLP, and (bottom right) T850 anomalies in ASO onto the lag –4 AMJ SST time series.

Z250 anomaly pattern (not shown) that resembled that derived from the MCA, with significance levels often nearly as high as in Fig. 7. Hence, both centers of action seem to influence the atmosphere. The maximum atmospheric response for each box is about 20 m K^{-1} at 250 mb. This is substantially smaller than in the MCA, which is not surprising since the SST estimates are based on box averaged values rather than the maximum, and the MCA maximizes the covariance. Note that this calculation is independent from the MCA, except for the choice of season and box location, suggesting that the MCA results are robust.

To investigate the feedback of the late summer atmospheric response onto the ocean, several oceanic forcing fields in ASO were regressed onto the AMJ SST time series. The regression of the surface wind stress (Fig. 8, top) shows a large eastward or northeastward wind stress anomaly in the northern part of the domain, a cyclonic anomaly off the U.S. western coast, and a small westward wind stress anomaly in the northern Tropics. The associated Ekman advection should contribute to cooling the SST to the north, thus reinforcing the northern lobe of the SST anomaly, and warm it in the northern Tropics, where it should damp the SST anomaly. The anomalous easterlies in the Tropics should also increase the strength of the subtropical cell, after adjustment.

Since the SST anomaly in Fig. 4 bears some similarity with the SVD3 SST pattern of Solomon et al. (2003, their Fig. 2) that is in part responsible for the decadal variability of the North Pacific subtropical cell in their model (see section 2), it is worth noting that our summer wind stress pattern is similar to their SVD3 wind stress pattern in the northern Tropics, but different at higher latitudes. Hence, our analysis does not support the air–sea feedbacks that they derived from contemporary correlations between SST and wind stress.

The ASO Ekman pumping is rather noisy and statistical significance is very low (not shown), so the summer signal should have little influence on the North Pacific gyre circulation. Finally, the ASO surface heat flux (Fig. 8, bottom) mostly acts as a negative feedback

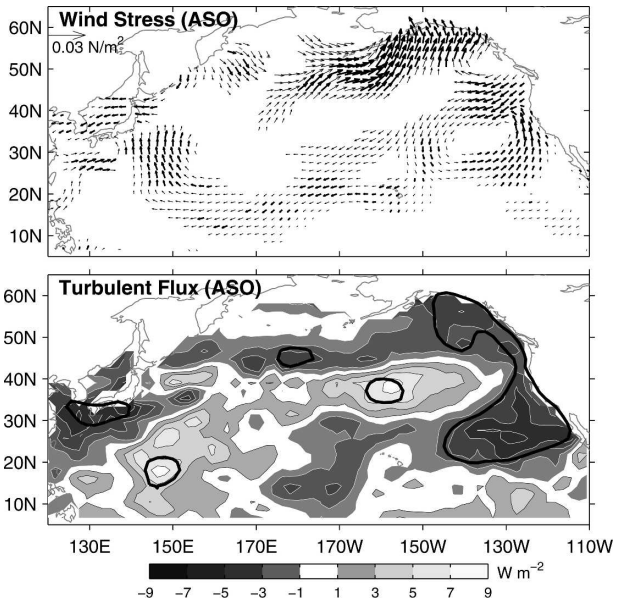

FIG. 8. Regression of (top) surface wind stress and (bottom) turbulent heat flux in ASO onto the lag –4 AMJ SST time series. White contours are for negative values and black contours for positive ones. The thick lines indicate the estimated 5% significance level. The wind stress is plotted in thin (thick) line when the correlation exceeds the estimated 20% (5%) significance level.

on the SST anomaly, as seen by the comparison with the ASO SST anomaly in Fig. 5 (bottom).

5. SST anomaly influence during late fall and early winter

To illustrate the signal found in late fall and early winter, we show in Fig. 9 the maximum covariance patterns for Z250 in NDJ and SST anomalies at all lags between –10 and 1 that are 20% significant in both SC and correlation. As before, the SC is strongest and most significant at lags 0 and 1, reflecting the forcing of the SST by the dominant atmospheric mode in the cold season, which is the Pacific–North American (PNA) pattern. Correspondingly, the SST pattern resembles the first SST anomaly EOF from OND to DJF, with a maximum amplitude along the sub-Arctic front near 40°N, and anomalies of the opposite sign around it.

When the ocean leads by 1 to 4 months (lags –1 to –4), the SC is lower but is still significant, as is the cross-validated correlation (Table 1), suggesting that the SST anomalies have a substantial influence on the large-scale atmospheric circulation. The maximum covariance patterns vary little with lag, except for an east-

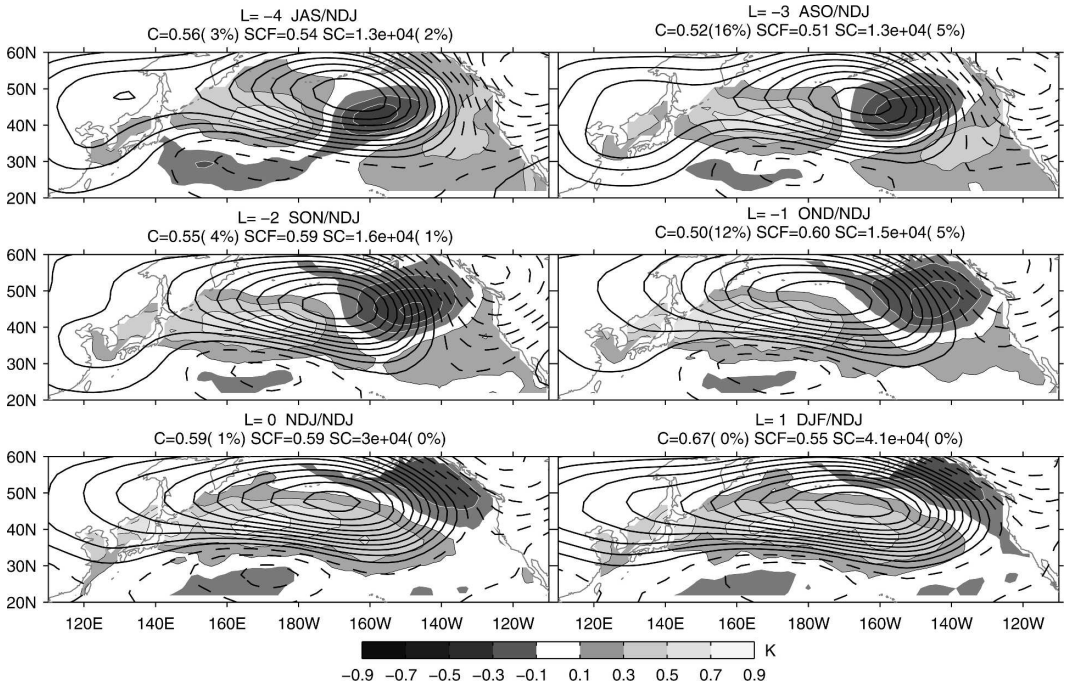

FIG. 9. Maximum covariance pattern for NDJ Z250 (contour interval: 6 m with negative values dashed) and SST (scale in K with white contours for negative values and black contours for positive ones) anomalies for the first mode between lag –4 (SST leads) and lag 1 (SST follows). The time series have been normalized so that the figure shows typical amplitudes. The correlation (C) between the MCA time series, the SC fraction (F), and the SC are given for each lag. The estimated significance levels are given in parentheses.

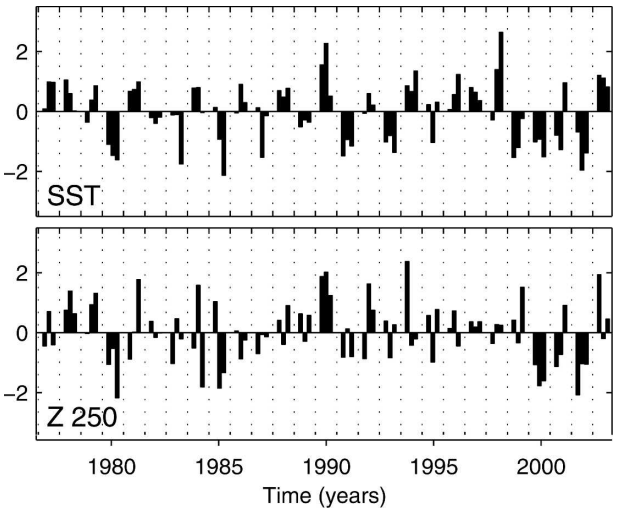

FIG. 10. Time series of the lag –4 MCA mode in Fig. 9 for (top) SST in JAS and (bottom) Z250 in NDJ. Each year is separated by a blank interval.

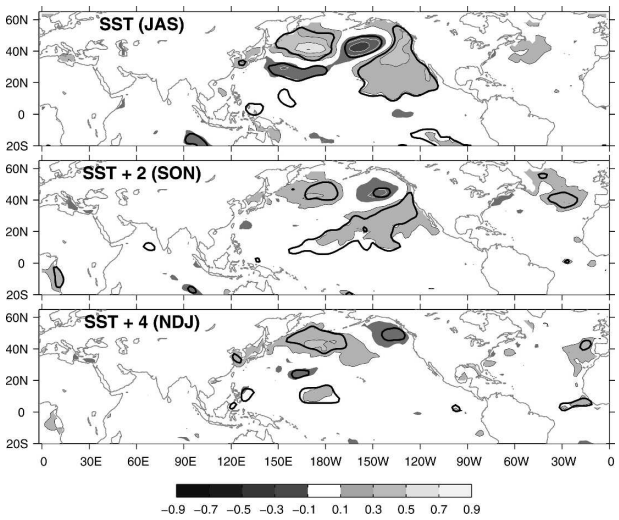

FIG. 11. Regression of the SST anomalies in (top) JAS, (middle) 2 months later in SON, and (bottom) 4 months later in NDJ onto the lag – 4 JAS SST time series shown in Fig. 10. White contours are for negative values and black contours for positive ones. The thick lines indicate the estimated 5% significance level.

ward propagation (or shift) of the SST anomaly. The latter is a quadripole with maximum amplitude along 40°N that does not directly correspond to a main summer or fall SST EOF. The atmospheric signal is large near the Aleutian center (up to 70 m K^{-1} at 250 mb) and PNA-like (see also Fig. 14 below), thus resembling the dominant atmospheric mode in the cold season, although the center of action over northwest Canada is shifted a bit southward and there is a weak secondary maximum over northeast Asia. This resemblance is consistent with Peng and Robinson (2001), who found that a GCM response to extratropical Pacific SST anomalies in winter tended to strongly resemble the main patterns of the model's natural variability.

Although the SC and the cross-validated correlation are maximum when SST leads by 2 months, we first focus on lag –4 (SST in JAS) as it leads to some predictability at longer range (Table 1). The two time series are rather noisy (Fig. 10), showing somewhat less (and different) low-frequency variability than in the summer case. Regression of the SST anomaly field in JAS (Fig. 11, top), SON (2 months later, middle), and NDJ (4 months later, bottom) onto the JAS SST time series indicates that the SST anomaly is primarily limited to the North Pacific, is quite persistent, and indeed propagates eastward, in particular between SON and NDJ when the initial quadripolar pattern has drastically changed shape and become a dipolar one. A similar change of shape is found when using the lag –2 MCA to define the SON SST time series. Note that it was again verified that the MCA mode is not related to changes in the equatorial Pacific when the ENSO signal is kept in the data.

The implied eastward propagation speed is faster than could be expected from oceanic advection, suggesting that the change of shape of the SST anomaly is primarily due to an active air–sea coupling. Indeed, the NDJ pattern is similar to the SST anomaly pattern found at lags 0 and 1 in Fig. 9, which represents the SST response to the PNA forcing and is also seen at lags 0 and 1 in late fall. The SST evolution in Fig. 11 could thus be mostly due to a PNA forcing that is associated with the atmospheric response to the JAS SST anomaly earlier in the fall. To support this hypothesis, we show in Fig. 12 the lag −2 MCA patterns between SST anomalies and Z250 anomalies in SON (top) and OND (bottom), when statistical significance is already high (see also Table 1). In both cases, there is a good resemblance with the patterns in Fig. 9, although Z250 is shifted a bit westward. Although these MCAs are not independent, they suggest that the SST anomaly is already forcing a PNA-like response in the fall. The atmospheric response could in turn act on the SST and contribute to its progressive change of shape, so that by NDJ the SST anomaly largely resembles that generated by the PNA pattern. Consistent with such an active air–sea coupling in the fall, the amplitude of the maximum SST covariance pattern (see Fig. 9) increases from lag – 4 (SST in JAS) to –2 (SST in SON). As the total SST anomaly variances start decreasing in the fall when the mixed layer deepens, the signal-to-noise ratio for the SST anomaly pattern that forces the PNA increases until SON. In the early winter case, the atmospheric predictability is thus highest when SST leads by 2

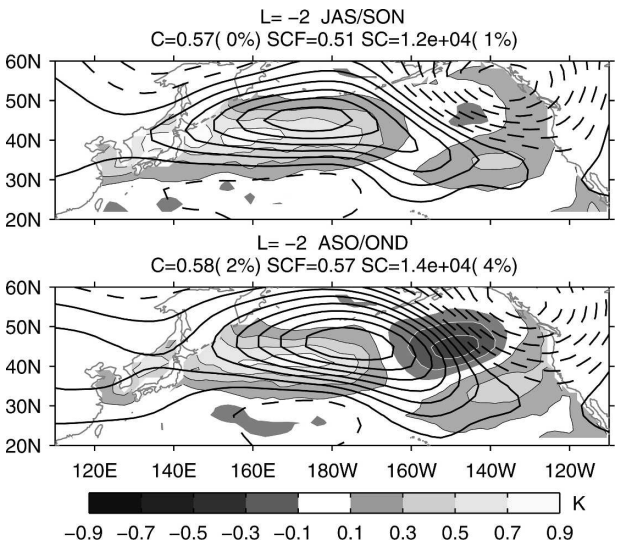

FIG. 12. Same as in Fig. 9, but for the lag –2 patterns when Z250 is taken in (top) SON and (bottom) OND.

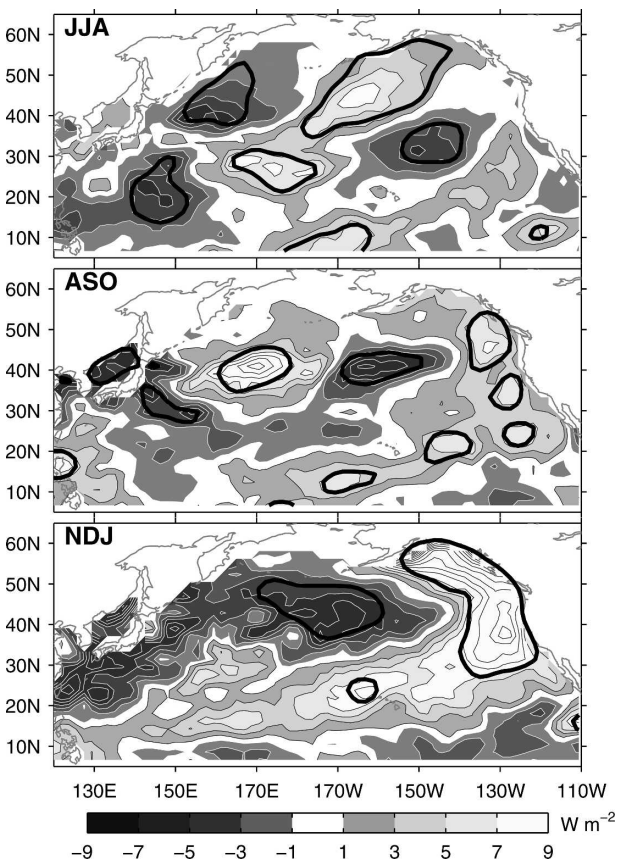

FIG. 13. Regression of the turbulent heat flux on the lag –4 JAS SST anomaly time series (top) 1 month before (JJA), (middle) 1 month after (ASO), and (bottom) 4 months later (NDJ). White contours are for negative values and black contours for positive ones. The thick lines indicate the estimated 5% significance level.

months (Table 1). Note that no significant relation is found in the MCAs between the PNA-like signal and SST anomalies taken before JAS (see also Fig. 2), which suggests that the SST anomaly that is responsible for the active coupling with the atmosphere only appears in summer.

Our interpretation is also consistent with the lead and lag relation between the SST anomaly in JAS and the surface turbulent heat flux anomalies (Fig. 13). When the turbulent heat flux leads by 1 month (top), its pattern suggests that it contributes to the generation of the JAS SST anomaly at midlatitude. On the other hand, there is little correspondence in the subtropics, where the surface radiation flux is likely to play a more important role. In ASO when the turbulent heat flux follows by 1 month (middle), it largely reflects the usual negative heat flux feedback, except off eastern Asia. In NDJ (bottom), the heat flux anomaly should be compared to the SST anomaly in Fig. 11 (bottom), which was also projected forward by 4 months. The correspondence between the two patterns is rather good, but the change of sign suggests that the heat flux is now reinforcing (or, in our interpretation, contributing to generating) the SST anomaly. It is shown (in Fig. 15 below) that anomalous Ekman advection also contributes to reinforcing the SST anomaly. Note that the heat flux cools the SST off the United States and in the subtropics, which could explain why the positive SST anomaly seen in this region in SON (Fig. 11, middle) has disappeared by NDJ. As the NDJ heat flux pattern in Fig. 13 is characteristic of that associated with the PNA pattern (Cayan 1992), the heat flux evolution supports the hypothesized interaction loop.

To discuss the hemispheric signature of the 250-mb signal in NDJ, we choose the MCA at lag –2, as the SC and the cross-validated correlation are the largest. Figure 14 confirms the resemblance of the tropospheric signal with the PNA, with a large Aleutian center of action, and centers of alternating sign over northwestern and southeastern North America, as well as in the subtropical North Pacific. The signal is largely equivalent barotropic, but the wavelike propagation is best seen in the middle and upper troposphere, while SLP is more strongly dominated by the high in the Aleutian region (for this SST polarity). There are strong and significant temperature anomalies over North America. The PNA pattern is robust and is also seen at lags –4, −3, and −1. On the other hand, the significance of the other centers of action such as those over the eastern Mediterranean or eastern Asia is depends somewhat on the lag and the level, suggesting less robustness.

To try determining whether the atmosphere is more

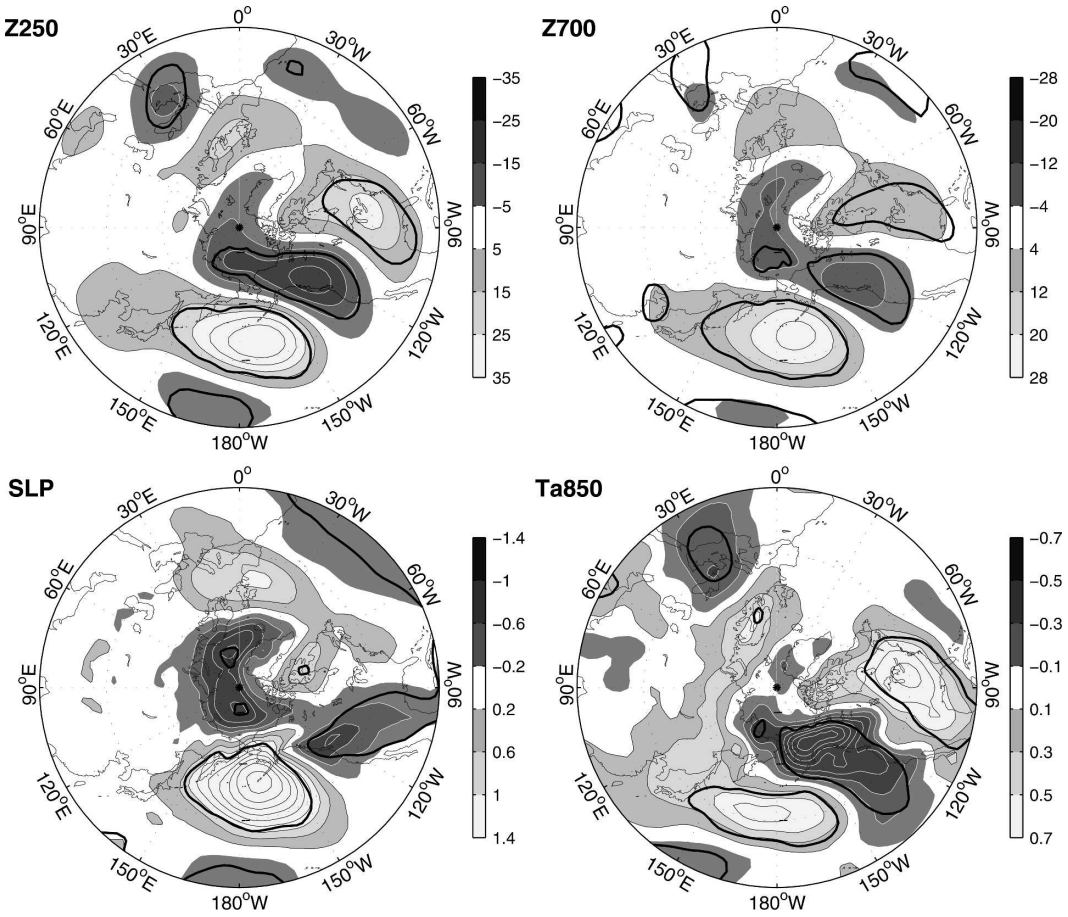

FIG. 14. Same as in Fig. 7, but in NDJ onto the lag –2 SON SST anomaly time series.

sensitive to a part of the SON SST anomaly pattern, we have constructed SST anomaly time series for three boxes centered on its main centers of action (see Fig. 9): 35°–45°N, 150°E–180°; 40°–50°N, 160°–140°W; 30°–40°N, 25°–35°N, 140°–120°W. Each box leads to a good hindcast of most of the PNA signal at 250 mb, although the center of action in the subtropical North Pacific is only significantly reproduced from the southwestern box. The amplitude of the Aleutian center of action is smaller than in the MCA, reaching about 35 m K^{-1} for each of the two northern boxes and 50 m K^{-1} for the southwestern one, which yields similar results since the SST anomaly is smaller. The significance and amplitude of the other centers of action is more variable, which confirms their lesser robustness.

The Ekman pumping and the surface wind stress anomalies associated with the NDJ atmospheric response (Fig. 15) are characteristic of the fields associated with the PNA pattern, with a strong anticyclonic circulation centered near the Aleutian low and Ekman pumping in the northern half of the domain, and a weaker cyclonic circulation centered around 25°N, 180° and an Ekman suction south of about 35°N (Ishi and Hanawa 2005). The strong easterlies along 40°N should reinforce the positive SST anomaly and extend it eastward via anomalous meridional Ekman advection, thus acting as a propagator like the surface heat flux. The Ekman pumping should decrease the climatological forcing and lead, after adjustment, to a slowdown of the subtropical and subpolar gyres. Yet, this should not substantially affect the SST anomaly in Fig. 11 (bottom) since SST along the subarctic front is largely controlled by local surface heat exchanges and Ekman advection (Seager et al. 2001; Nakamura and Kazmin 2003). Hence, there is no clear indication of a delayed dynamical feedback on the SST, as in the Latif and Barnett's (1994) scenario. Note finally that the surface wind stress associated with the winter signal is eastward in the northern Tropics, which should decrease the strength of the subtropical cell, after adjustment. However, there is little resemblance with the SST and wind stress patterns discussed in Solomon et al. (2003).

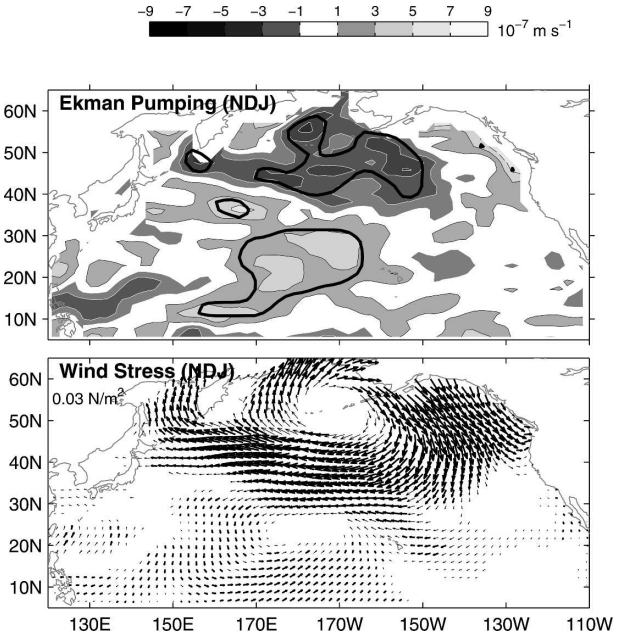

FIG. 15. Regression of the (top) Ekman pumping and (bottom) surface wind stress in NDJ on the lag –2 SON SST anomaly time series. White contours are for negative values and black contours for positive ones. The thick lines indicate the estimated 5% significance level. The wind stress is plotted in thin (thick) line when the correlation exceeds the estimated 20% (5%) significance level.

6. Discussion and conclusions

The results from the lagged MCA, confirmed by regression analysis, suggest that North Pacific SST anomalies influence the large-scale atmospheric circulation during two seasons, late summer and late fall–early winter. This influence is unrelated to the ENSO teleconnections, which were removed prior to the analysis, and it should not be affected by trends and low frequencies, which were also removed. However, the evidence for an SST anomaly influence on the atmosphere was stronger in the 1977–2003 period that forms the basis of the present analysis than during the first half of the NCEP–NCAR reanalysis. This is in part due to the better data quality but is also linked to the climate shift of the mid-1970s. Liu et al. (2006) have recently found in an independent, but similar, study that during the 1958–93 period, the summer atmosphere was responding earlier (in JJA) and differently to previous North Pacific SST anomalies, while no signal was detected later in the year.

In both seasons, the atmospheric signal is hemispheric in extent. It is significantly related to North Pacific SST anomalies up to at least 4 or 5 months before. This does not imply that the SST forcing occurs that much in advance but reflects the large persistence of the SST anomalies and, perhaps, a somewhat longer atmospheric response time than is usually assumed (Ferreira and Frankignoul 2005).

The late summer signal is primarily found in ASO when the land–sea thermal contrast has become small. It is most significant in the middle and upper troposphere, and it can be linked to spring SST anomalies resembling the main mode of interannual SST variability in the North Pacific between winter and summer, with a broad maximum along 35°N and anomalies of the opposite sign around it. As shown by considering the lead and lag relation between the spring SST anomaly and the surface turbulent heat flux, the SST anomaly is mostly generated by anomalous air–sea heat exchanges, except near the Kuroshio and its extension where oceanic advection plays a role (Qiu 2000). The variability of the Kuroshio Extension, which is itself remotely wind driven, probably explains the decadal variability of the SST anomaly time series since the 1990s. The atmospheric signal is largest when SST is in AMJ and precedes by 4 months, presumably because the SST anomaly that influences the late summer atmosphere only slowly decays throughout the summer while its signal-to-noise ratio decreases, as other SST patterns are efficiently generated by the atmosphere when the mixed layer is shallow. The atmospheric response is significant over the North Pacific, North America, Europe, and eastern Asia. It is primarily equivalent barotropic, but there is some baroclinicity in the western North Pacific, with a high above the Kuroshio Extension region that tilts westward with height. The amplitude of the response at 250 mb reaches 35 m K^{-1} in the MCA (a likely overestimate) and 20 m K^{-1} in the regression on SST anomalies in two boxes located near the centers of action of the MCA SST anomaly pattern. As estimated by the square of the cross-validated correlation between the MCA time series, 29% of the variance of the monthly atmospheric anomaly pattern at 250 mb can be forecasted in ASO from the SST anomaly 4 months earlier. Useful short-time-scale climate predictability should thus result in late summer from the lagged relations established here.

A more persistent oceanic influence on the atmosphere is taking place in fall and early winter. The atmospheric response resembles the PNA pattern and peaks in NDJ, but it is already recognized in OND, and even in SON, albeit slightly shifted westward. The SST anomaly in JAS is a quadripole. It is rather persistent but propagates eastward, progressively transforming itself into the bipolar SST pattern that characterizes the SST response to forcing by the PNA pattern. Some evidence was found that the SST anomaly evolution is

due in part to the back interaction via surface heat flux and Ekman advection of the PNA-like response onto the SST, suggesting that an active air–sea coupling takes place throughout the fall. Correspondingly, the SC, the correlation, and the statistical significance are largest at lag –2 (SST in SON). The maximum atmospheric response occurs over the Aleutian center, reaching 70 m K^{-1} in the MCA but about 35 m K^{-1} in the regression onto the two main SST anomaly poles. Again, some climate predictability is expected from the lagged relationships established here. The 2-month forecast skill of the PNA-like signal in the MCA is 18%, and the 4-month one is 13%. Although these figures are smaller than in the summer case, presumably because of the larger atmospheric variability in winter, they should lead to useful forecasts since the PNA pattern is the dominant winter mode in the North Pacific.

The large persistence of the North Pacific SST anomalies from summer to the next winter and their eastward propagation were discussed by Zhang et al. (1998), although their dominant summer pattern differed east of the date line from our JAS SST pattern. Norris et al. (1998) suggested that a positive feedback between low clouds and SST in summertime could contribute to the large SST anomaly persistence, and Zhang et al. (1998) even speculated that the SST anomaly at the onset of the winter season could trigger a PNA response, consistent with the present findings

That the North Pacific SST anomalies only significantly influence the large-scale atmospheric circulation during certain seasons is consistent with the North Atlantic case (Czaja and Frankignoul 1999, 2002), as well as with GCM sensibility studies where the atmospheric response to prescribed SST anomalies strongly depends on the climatological flow, which can change substantially from one month to the next (Peng et al. 1997). A direct comparison with GCM response studies is difficult, however, since the SST influence onto the atmosphere is detected either in late summer or in late fall–early winter but disappears in DJF, while most GCM studies focus on SST forcing during January or February.

Because in several climate scenarios it has been assumed that an active air–sea coupling in the North Pacific was contributing to decadal variability, we have also discussed the surface fluxes that are associated with the atmospheric response. In both seasons, we found no convincing evidence that the Ekman pumping could alter after adjustment the strength of the subtropical and subpolar gyres in a way that would feed back on the SST anomaly that generated the atmospheric response. Hence, our analysis seems inconsistent with the delayed negative feedback hypothesized by Latif and Barnett (1994), and more in tune with the lack of significant dynamical feedback found by Schneider et al. (2002). Note that the surface heat flux mostly acts as a negative feedback, as discussed in Frankignoul and Kestenare (2002). Also noteworthy is that in both seasons the atmospheric response to the SST anomalies shows significant changes in the zonal wind stress in the northern Tropics, which may affect the strength of the Pacific subtropical cells. However, the patterns differ from those derived from contemporary correlations by Solomon et al. (2003), which were responsible for the decadal variability of the subtropical cells in their model.

In this paper, we have focused on detecting the influence of the North Pacific SST anomalies on the large-scale atmospheric circulation. Such influence should involve the diabatic heating due to the air–sea heat exchanges, wave propagation, the storm track, and the interaction between the synoptic eddies and the large-scale flow, but in a way that remains to be established.

Acknowledgments. We thank E. Kestenare for her contribution to the early stages of the analysis and the reviewers for useful comments. The NCEP–NCAR reanalysis data were provided through the NOAA Climate Center (http://www.cdc.noaa.gov/). This work was supported by the EU Framework 6 Programme under Contract 003903-GOCE (DYNAMITE) and by the Institut Universitaire de France.

REFERENCES

Barnett, T. P., 1981: Statistical prediction of North American air temperature from Pacific predictors. *Mon. Wea. Rev.,* **109,** 1021–1041.

Bretherton, C. S., C. Smith, and J. M. Wallace, 1992: An intercomparison of methods for finding coupled patterns in climate data. *J. Climate,* **5,** 541–560.

——, M. Widman, V. P. Dymnikov, J. M. Wallace, and I. Bladé, 1999: The effective number of spatial degrees of freedom of a time-varying field. *J. Climate,* **12,** 1990–2009.

Cassou, C., C. Deser, L. Terray, J. W. Hurrell, and M. Drévillon, 2004: Summer sea surface temperature conditions in the North Atlantic and their impact upon the atmospheric circulation in early winter. *J. Climate,* **17,** 3349–3363.

Cayan, D. R., 1992: Latent and sensible heat flux anomalies over the northern oceans: The connection to monthly atmospheric circulation. *J. Climate,* **5,** 354–369.

Cheng, X., and T. J. Dunkerton, 1995: Orthogonal rotation of spatial patterns derived from singular value decomposition analysis. *J. Climate,* **8,** 2631–2643.

Czaja, A., and C. Frankignoul, 1999: Influence of the North Atlantic SST on the atmospheric circulation. *Geophys. Res. Lett.,* **26,** 2969–2972.

——, and ——, 2002: Observed impact of Atlantic SST anomalies on the North Atlantic oscillation. *J. Climate,* **15,** 606–623.

Davis, R. E., 1976: Predictability of sea surface temperature and sea level pressure anomalies over the North Pacific Ocean. *J. Phys. Oceanogr.,* **6,** 249–266.

——, 1978: Predictability of sea level pressure anomalies over the North Pacific Ocean. *J. Phys. Oceanogr.,* **8,** 233–246.

Ferreira, D., and C. Frankignoul, 2005: The transient atmospheric response to midlatitude SST anomalies. *J. Climate,* **18,** 1049–1067.

Frankignoul, C., 1985: Sea surface temperature anomalies, planetary waves and air–sea feedback in the middle latitudes. *Rev. Geophys.,* **23,** 357–390.

——, and K. Hasselmann, 1977: Stochastic climate models. II: Application to sea-surface temperature variability and thermocline variability. *Tellus,* **29,** 284–305.

——, and E. Kestenare, 2002: The surface heat flux feedback. Part I: Estimates from observations in the Atlantic and the North Pacific. *Climate Dyn.,* **19,** 633–647.

——, A. Czaja, and B. L'Heveder, 1998: Air–sea feedback in the North Atlantic and surface boundary conditions for ocean models. *J. Climate,* **11,** 2310–2324.

Horel, J. D., and J. M. Wallace, 1981: Planetary-scale atmospheric phenomena associated with the interannual variability of sea surface temperature in the equatorial Pacific. *Mon. Wea. Rev.,* **109,** 813–829.

Ishi, Y., and K. Hanawa, 2005: Large-scale variabilities of wintertime wind stress curl field in the North Pacific and their relation to atmospheric teleconnection patterns. *Geophys. Res. Lett.,* **32,** L10607, doi:10.1029/2004GL022330.

Kalnay, E., and Coauthors, 1996: The NCEP/NCAR 40-Year Reanalysis Project. *Bull. Amer. Meteor. Soc.,* **77,** 437–471.

Kushnir, Y., W. A. Robinson, I. Bladé, N. M. J. Hall, S. Peng, and R. Sutton, 2002: Atmospheric GCM response to extratropical SST anomalies: Synthesis and evaluation. *J. Climate,* **15,** 2233–2256.

Latif, M., and T. P. Barnett, 1994: Causes of decadal climate variability over the North Pacific and North America. *Science,* **266,** 634–637.

Lau, K.-M., K.-M. Kim, and S. Chen, 2002: Potential predictability of seasonal precipitation over the United States from canonical ensemble correlation predictions. *Geophys. Res. Lett.,* **29,** 1097, doi:10.1029/2001GL014263.

Liu, Q., N. Wen, and Z. Liu, 2006: An observational study of the impact of the North Pacific SST on the atmosphere. *Geophys. Res. Lett.,* **33,** L18611, doi:10.1029/2006GL026082.

Liu, Z., and L. Wu, 2004: Atmospheric response to North Pacific SST: The role of ocean–atmosphere coupling. *J. Climate,* **17,** 1859–1882.

Nakamura, H., and A. S. Kazmin, 2003: Decadal changes in the North Pacific oceanic frontal zones as revealed in ship and satellite observations. *J. Geophys. Res.,* **108,** 3078, doi:10.1029/1999JC000085.

Namias, J., 1963: Large-scale air–sea interactions over the North Pacific from summer 1962 through the subsequent winter. *J. Geophys. Res.,* **68,** 6171–6186.

——, 1976: Negative ocean–air feedback systems over the North Pacific in the transition from warm to cold seasons. *Mon. Wea. Rev.,* **104,** 1107–1121.

Nonaka, M., and S.-P. Xie, 2003: Covariations of sea surface temperature and wind over the Kuroshio and its extension: Evidence for ocean-to-atmosphere feedback. *J. Climate,* **16,** 1404–1413.

Norris, J. R., Y. Zhang, and J. M. Wallace, 1998: Role of low clouds in summertime atmosphere–ocean interactions over the North Pacific. *J. Climate,* **11,** 2482–2490.

Peng, S., and J. S. Whitaker, 1999: Mechanisms determining the atmospheric response to midlatitude SST anomalies. *J. Climate,* **12,** 1393–1408.

——, and W. A. Robinson, 2001: Relationships between atmospheric internal variability and the response to an extratropical SST anomaly. *J. Climate,* **14,** 2943–2959.

——, ——, and M. P. Hoerling, 1997: The modeled atmospheric response to midlatitude SST anomalies and its dependence on background circulation states. *J. Climate,* **10,** 971–987.

Qiu, B., 2000: Interannual variability of the Kuroshio Extension and its impact on the wintertime SST field. *J. Phys. Oceanogr.,* **30,** 1486–1502.

——, 2003: Kuroshio Extension variability and forcing of the Pacific decadal oscillation: Responses and potential feedback. *J. Phys. Oceanogr.,* **33,** 2465–2482.

Schneider, N., A. J. Miller, and D. W. Pierce, 2002: Anatomy of North Pacific decadal variability. *J. Climate,* **15,** 586–605.

Seager, R., Y. Kushnir, N. H. Naik, M. A. Cane, and J. Miller, 2001: Wind-driven shifts in the latitude of the Kuroshio–Oyashio Extension and generator of SST anomalies on decadal time scales. *J. Climate,* **14,** 4249–4265.

Solomon, A., J. P. McCreary, R. Kleeman, and B. A. Klinger, 2003: Interannual and decadal variability in an intermediate coupled model of the Pacific region. *J. Climate,* **16,** 383–405.

Straus, D. M., and J. Shukla, 2002: Does ENSO force the PNA? *J. Climate,* **15,** 2340–2358.

Tanimoto, Y., H. Nakamura, T. Kagimoto, and S. Yamane, 2003: An active role of extratropical sea surface temperature anomalies in determinant anomalous turbulent heat flux. *J. Geophys. Res.,* **108,** 3304, doi:10.1029/2002JC001750.

Trenberth, K. E., and J. W. Hurrell, 1994: Decadal atmosphere–ocean variations in the Pacific. *Climate Dyn.,* **9,** 303–319.

Zhang, Y., J. R. Norris, and J. M. Wallace, 1998: Seasonality of large-scale atmosphere–ocean interaction over the North Pacific. *J. Climate,* **11,** 2473–2481.